



**HAL**  
open science

## Processing strategy for reduced energy demand of nanostructured CNF/clay composites with tailored interfaces

Xuan Yang, Lengwan Li, Yoshiharu Nishiyama, Michael Reid, Lars Berglund

► **To cite this version:**

Xuan Yang, Lengwan Li, Yoshiharu Nishiyama, Michael Reid, Lars Berglund. Processing strategy for reduced energy demand of nanostructured CNF/clay composites with tailored interfaces. Carbohydrate Polymers, 2023, 312, pp.120788. 10.1016/j.carbpol.2023.120788 . hal-04177332

**HAL Id: hal-04177332**

**<https://hal.science/hal-04177332>**

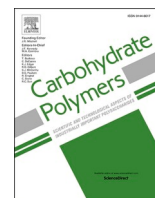
Submitted on 4 Aug 2023

**HAL** is a multi-disciplinary open access archive for the deposit and dissemination of scientific research documents, whether they are published or not. The documents may come from teaching and research institutions in France or abroad, or from public or private research centers.

L'archive ouverte pluridisciplinaire **HAL**, est destinée au dépôt et à la diffusion de documents scientifiques de niveau recherche, publiés ou non, émanant des établissements d'enseignement et de recherche français ou étrangers, des laboratoires publics ou privés.



Distributed under a Creative Commons Attribution 4.0 International License



# Processing strategy for reduced energy demand of nanostructured CNF/clay composites with tailored interfaces

Xuan Yang<sup>a,b</sup>, Lengwan Li<sup>b,\*</sup>, Yoshiharu Nishiyama<sup>c</sup>, Michael S. Reid<sup>d,e</sup>, Lars A. Berglund<sup>b,\*</sup>

<sup>a</sup> State Key Lab of Chemical Engineering, Key Laboratory of Biomass Chemical Engineering of Ministry of Education, College of Chemical and Biological Engineering, Zhejiang University, Hangzhou 310027, PR China

<sup>b</sup> Wallenberg Wood Science Center, Department of Fibre and Polymer Technology, KTH Royal Institute of Technology, Teknikringen 56–58, Stockholm SE-100 44, Sweden

<sup>c</sup> Univ. Grenoble Alpes, CNRS, CERMAV, 38000 Grenoble, France

<sup>d</sup> Division of Fibre technology, Department of Fibre and Polymer Technology, KTH Royal Institute of Technology, Teknikringen 56–58, SE-100 44 Stockholm, Sweden

<sup>e</sup> RISE Research Institutes of Sweden, Drottning Kristinas väg 55, SE-114 28 Stockholm, Sweden

## ARTICLE INFO

### Keywords:

CNF/clay biocomposites  
Cumulative energy demand  
Fibrillation  
Exfoliation  
XRD

## ABSTRACT

Nacre-mimicking nanocomposites based on colloidal cellulose nanofibrils (CNFs) and clay nanoparticles show excellent mechanical properties, yet processing typically involves preparation of two colloids followed by a mixing step, which is time- and energy-consuming. In this study, a facile preparation method using low energy kitchen blenders is reported in which CNF disintegration, clay exfoliation and mixing carried out in one step. Compared to composites made from the conventional method, the energy demand is reduced by about 97 %; the composites also show higher strength and work to fracture. Colloidal stability, CNF/clay nanostructure, and CNF/clay orientation are well characterized. The results suggest favorable effects from hemicellulose-rich, negatively charged pulp fibers and corresponding CNFs. CNF disintegration and colloidal stability are facilitated with substantial CNF/clay interfacial interaction. The results show a more sustainable and industrially relevant processing concept for strong CNF/clay nanocomposites.

## 1. Introduction

Nacre, a natural nanocomposite with oriented inorganic platelets and soft organic “glue” matrix has favorable mechanical properties in terms of stiffness, strength and toughness (Gim et al., 2019). Researchers have developed different material combinations and different processing methods to mimic such brick-and-mortar structures (Luz & Mano, 2009; Zhang, Tian, Zhong, & Shi, 2018). Among these, nanocomposites based on wood cellulose nanofibrils (CNFs) and montmorillonite (MTM) stand out due to abundant availability and excellent mechanical properties (Young’s modulus >30 GPa and ultimate strength >200 MPa) (Liu, Walther, Ikkala, Belova, & Berglund, 2011; Medina et al., 2019).

There are many advantages for choosing CNF and MTM. CNFs based on the elementary reinforcing components in the wood cell wall, can be disintegrated from wood pulp fibers to the form of hydrocolloidal particles (Chen et al., 2020). They have unique character as a polymer matrix including nanoscale dimensions (widths around 4–10 nm and lengths of 0.5–2 μm), ability to form strong, dense and ductile network

structure, as well as CNF surface modification potential (Kontturi et al., 2018; Vanderfleet & Cranston, 2021). MTM is one of the most common natural clay silicate minerals with layered structure. With an in-plane modulus of 170–270 GPa (Manevitch & Rutledge, 2004), aspect ratio above 200 (1 nm thickness, 200 nm -1 μm lateral dimension) as well as low pH sensitivity and high thermal stability, MTM is an excellent “brick” in nacre-mimetic nanocomposites (Bee, Abdullah, Bee, Sin, & Rahmat, 2018; Carosio, Kochumalayil, Cuttica, Camino, & Berglund, 2015; Zhou et al., 2022).

Early work on wood CNF/clay nacre-mimetic nanocomposites was carried out in our laboratory (Li et al., 2022; Andong Liu & Berglund, 2012) and high mechanical, gas barrier and fire retardancy properties were combined with high optical transmittance. The “conventional” preparation route, called *Ref* method in the following, normally consists of preparation of CNF hydrocolloids by disintegration of chemical wood pulp, MTM exfoliation into hydrocolloid, mixing of the two colloids, filtration and drying in order to achieve ideally structured composite films: 1) thin MTM (or even mono layered) with the possibility of high

\* Corresponding authors.

E-mail addresses: [lengwan@kth.se](mailto:lengwan@kth.se) (L. Li), [blund@kth.se](mailto:blund@kth.se) (L.A. Berglund).

<https://doi.org/10.1016/j.carbpol.2023.120788>

Received 31 December 2022; Received in revised form 1 March 2023; Accepted 4 March 2023

Available online 11 March 2023

0144-8617/© 2023 The Authors. Published by Elsevier Ltd. This is an open access article under the CC BY license (<http://creativecommons.org/licenses/by/4.0/>).

content (up to 80 wt%), 2) uniform dispersion of MTM within CNF matrix, and 3) preferred in-plane orientation (parallel to film surface) of both CNFs and MTM. To achieve this, pretreatments such as cation exchange have been used to improve MTM exfoliation, or surface modification to improve colloidal stability (Gao et al., 2019; Guo, Liu, Gates, & Zhou, 2020). Regarding CNFs, the preparation of colloidal stable CNFs of fine diameter is important. In most studies, TEMPO mediated oxidation of the chemical pulp fibers is used, followed by a high energy disintegration process using a homogenizer (Saito, Kimura, Nishiyama, & Isogai, 2007). Centrifugation is often used to remove larger clay particles and pulp fiber fragments, which further increases process energy demand.

Since the smallest possible CNF diameter is 3–4 nm, it is in practice not possible to fully cover a 1 nm thick MTM platelet with CNF, especially at high MTM content. There will also be small scale porosity associated with MTM tactoids. These factors impede stress transfer from CNF to MTM and the reinforcement efficiency is reduced at higher MTM content. Polymers have been added to the CNF/MTM mixtures, such as chitosan (Liu & Berglund, 2012), polyvinyl alcohol (PVA) (Wang, Cheng, Lin, & Jiang, 2014) and xyloglucan (Carosio, Medina, Kochumalayil, & Berglund, 2021), primarily to increase ductility. This, however, requires an additional step to adsorb polymer to either CNF or MTM prior to final mixing. Previously, holocellulose CNFs (Holo-CNFs) with high surface content of sorbed anionic hemicellulose were prepared by mild wood delignification followed by facile disintegration using low energy kitchen blenders (Yang, Jungstedt, Reid, & Berglund, 2021; Yang, Reid, Olsen, & Berglund, 2020). The unique hemicellulose shell layer on such Holo-CNFs may serve as a binder to improve the CNF/MTM interface.

Here, a simplified process route is reported for CNF/MTM composites where the process energy is reduced and the CNF/MTM interface is tailored. Instead of first preparing fine CNFs and MTM nanoplatelets separately, holocellulose wood fibers and raw MTM particles were mechanically mixed together, denoted *Premix* process in the following, in which CNF disintegration and MTM exfoliation take place simultaneously. The mixture is directly processed into composite films. The hypothesis is that energy cost can be reduced if CNF disintegration and MTM exfoliation take place simultaneously, and if MTM can still be well dispersed with preserved mechanical properties. The CNF/MTM composites from this new *Premix* process route show improved mechanical properties compared with CNF/MTM from the *Ref* process. The Young's modulus is 30 GPa, and ultimate strength is ~240 MPa at 50 wt% clay content. The fracture surfaces and nanostructures are characterized, the effect of hemicelluloses is discussed, and the total processing energy is estimated. With low energy demand, high mechanical properties and better understanding of processing-structure-property relationships, this work can contribute to industrial activities on related materials.

## 2. Experimental section

### 2.1. Sample preparation

#### 2.1.1. CNF preparation

**Holocellulose Fibers (Holo-Fibers)** were obtained using a mild peracetic acid (PAA) delignification on *Picea Abies* spruce according to previously published method (Yang, Berthold, & Berglund, 2019; Yang et al., 2020). Briefly, spruce was treated with PAA (4 wt%, pH 4.8 before reaction, 85 °C) until no visible yellow/brown color can be seen. Treated spruce was washed with 0.01 M NaOH and then extensively with deionized water to remove residual chemicals before further use. **Fine Holo-CNFs** were obtained by the disintegration of Holo-Fibers using a kitchen blender (Bosch SilentMixx Pro) (Yang et al., 2021). Large non-fibrillated fragments were removed using centrifugation at 4500 rpm for 15 min. **Enzymatic pretreated CNF (Enz-CNF)** were obtained by carried out a mild enzymatic pretreatment (Henriksson, Henriksson, Berglund, & Lindström, 2007) followed by the same disintegration

process for making Holo-CNFs. According to our previous investigation (Yang et al., 2020), the hemicellulose content of coarse Holo-CNF, fine Holo-CNF and Enz-CNF is 28.8 %, 26.4 % and 12.5 %, respectively. Enz-CNF has a low surface charge below 100  $\mu\text{equiv/g}$  whereas both Holo-CNFs have a surface charge of 200–230  $\mu\text{equiv/g}$ .

#### 2.1.2. MTM preparation

Fine MTM were obtained through several cycles of sonication and centrifugation at 4500 rpm for 30 min. The raw MTM (Na-Cloisite, BYK Additives, Germany) was kindly supplied by Bjørn Thorsen AB, which has a nominal density of 2.86 g/cm<sup>3</sup>.

#### 2.1.3. CNF/MTM mixture preparation

**Premix:** Certain amount of raw MTM (20, 30 and 50 wt%) was added into Holo-Fiber dispersion (~5 wt%). Then the mixture was blended using a kitchen blender (Blender Bosch SilentMixx Pro) at “high speed” setting. Deionized water was added to dilute the fibrillation “gel” every 15 s, until the final mixture has a CNF concentration ~ 0.3 wt%. In total, ~90 s of blending is applied. Note that no centrifugation is applied for *Premix* dispersion for following film preparation process. In order to determine the final yield of the nanoscale particles of the *Premix* dispersions, the dispersions were centrifugation at 4500 rpm for 15 min, the unfibrillated sediments were removed and the upper phase (nanoscale materials) was collected. The final yield of the nanoscale particle in coarse Holo-CNF (*Premix* 0), *Premix* 20, *Premix* 30 and *Premix* 50 samples is about 55, 64, 73, 73 wt%, respectively. *Ref:* As comparison, a conventional mixing method was also used following previous publications (Li et al., 2022; Medina et al., 2019): fine CNFs and fine MTM were mixed using ULTRA-TURRAX mixer at 12,000 rpm for 5 min.

#### 2.1.4. Nanocomposite film preparation

Cellulose MTM mixture suspension was diluted to 0.1 wt% under the mixing of Ultra-turrax mixer (IKA T25, Germany) at 12,000 rpm for 2 min. The suspension was filtered by an assembled fritted glass setup (Fig. S1) and polyvinylidene fluoride (PVDF) membrane filter with a pore size of 0.65  $\mu\text{m}$ . The filtration time is increase with MTM content, from 6 to 12 h for *Ref* samples, whereas it is shorter for *Premix* samples (5–6 h). The obtained wet cakes were dried in a paper sheet-forming equipment (Rapid Köthen) under vacuum (ca. 70 mbar) at 93 °C for 12 min. Note the films prepared by filtration and subsequent rapid dry has short preparation time, and also show better mechanical properties as suggested by previous study (Alves et al., 2022).

## 2.2. Characterizations

### 2.2.1. Tensile testing

The tensile mechanical properties were determined using an Instron 5944 with a 500 N load cell and a video extensometer. The specimen width and testing gauge length were set to 5 mm and 25 mm, respectively. Prior to testing, all the samples were conditioned at a relative humidity of 50 % and room temperature for at least 2 days.

### 2.2.2. Surface scanning microscopy

The fracture surfaces of nanocomposite films after tensile tests were imaged by field-emission scanning electron microscope (SEM, Hitachi S-4300, Japan), with 2–3 nm of palladium sputtering coating (Cressington 208HR).

### 2.2.3. Wide-angle X-ray diffraction

The in-plane orientation of CNFs within the composite films was quantified by wide-angle X-ray diffraction (WAXD, D8 VENTURE, USA, Mo-tube). The degree of orientation (*I*) was calculated as  $I = (180 - \text{FWHM})/180$ , where FWHM is the full width at half maximum of cellulose 200 peak azimuthal intensity distribution based on a Gaussian peak fitting. The stacking of clay is quantified from the MTM peak with  $q = 2 \text{ \AA}^{-1}$  using Scherrer equation (Hajizadeh, Taheri-Ledari, & Asl,

2022; Scherrer, 1918).

#### 2.2.4. UV-vis spectroscopy

The colloidal stability of the dispersions (0.05 wt%) and total transmittance of the composite films was characterized by UV-vis spectrum (UV-2550 Shimadzu spectrophotometer).

#### 2.2.5. Dynamic light scattering

The Zetasizer ZSU3205 instrument from Malvern Instruments was utilized for size and zeta potential measurement of the CNF and CNF/MTM dispersions in water with the concentration of  $\sim 0.05$  wt% at pH  $\sim 6.5$ . Fig. S3 shows some examples of the size and zeta potential distribution curves.

#### 2.2.6. Total porosity measurement

The total porosity was calculated based on the following equation:

$$\text{Total porosity} = 1 - \rho^* / \rho_s \quad (1)$$

where  $\rho_s$  is the theoretical composite density, using  $1.6 \text{ g/cm}^3$  for CNF,  $2.86 \text{ g/cm}^3$  for MTM.  $\rho^*$  is the measured bulk density based on weight and volume measurement. The films were cut into  $1.5 \times 1.5 \text{ cm}$  square to determine the weight and volume, 3 specimens of each sample were prepared. The thickness was measured by a Mitutoyo thickness gauge.

#### 2.2.7. Thermogravimetric analysis

The Thermogravimetric Analysis of prepared CNF/MTM nanocomposite films was performed via TGA (Mettler Toledo) under nitrogen atmosphere. The sample with a weight of  $\sim 3.5 \text{ mg}$  was placed in an aluminum oxide cylindrical crucible and heated from  $30$  to  $810 \text{ }^\circ\text{C}$  using a heating rate of  $10 \text{ }^\circ\text{C/min}$ .

#### 2.2.8. Energy demand calculation

Embodied energy cost was estimated based on the energy consumption per film ( $0.2 \text{ g}$ ) in each processing step. The power of processing machines during operation were measured by an energy meter (ESIC Technology LTD), which can measure the power and energy cost with a precision of  $1 \text{ watt}$  and  $0.01 \text{ kWh}$ , respectively. Note that ultra-turrax mixing and sonication has low power consumption, so that we used the working power (listed on the machine screen) and running time to do the calculation. We listed the working power of each step here: kitchen blender ( $0.398 \text{ kW}$ ), ultra-turrax ( $0.05 \text{ kW}$ ), centrifugation ( $1.47 \text{ kW}$ ), sonication ( $0.07 \text{ kW}$ ), and microfluidizer ( $3.7 \text{ kW}$ ). The operation time of each machine was based on the experimental demand. Note that the energy cost of filtration/dewatering process is also very important. In the present study, the dewatering time for different CNF nanopaper films are different:  $6 \text{ h}$  for *Premix* 50 and  $12 \text{ h}$  for *Ref* 50. Although the absolute energy cost here cannot be determined due to some technique issues, it agrees with the final conclusion that *Premix* method costs less energy compared to *Ref* method.

### 3. Results and discussion

Most previous investigations used two dispersions of pre-made fine CNF and fine clay (MTM) hydrocolloids which are mixed together before filtering and drying to form nanocomposite films (Li et al., 2022; Medina et al., 2019); this approach is the reference method termed “*Ref*” in Fig. 1. The main justification for this approach has been to ensure fine nanostructure in the final composite. Here, a different strategy termed “*Premix*” was developed in which crude MTM powder and Holo-Fiber pulp suspensions in water were mechanically mixed in a kitchen blender. Beyond simple mixing, Holo-Fibers were successfully disintegrated into fine CNFs with widths of  $4\text{--}10 \text{ nm}$ , and raw MTM

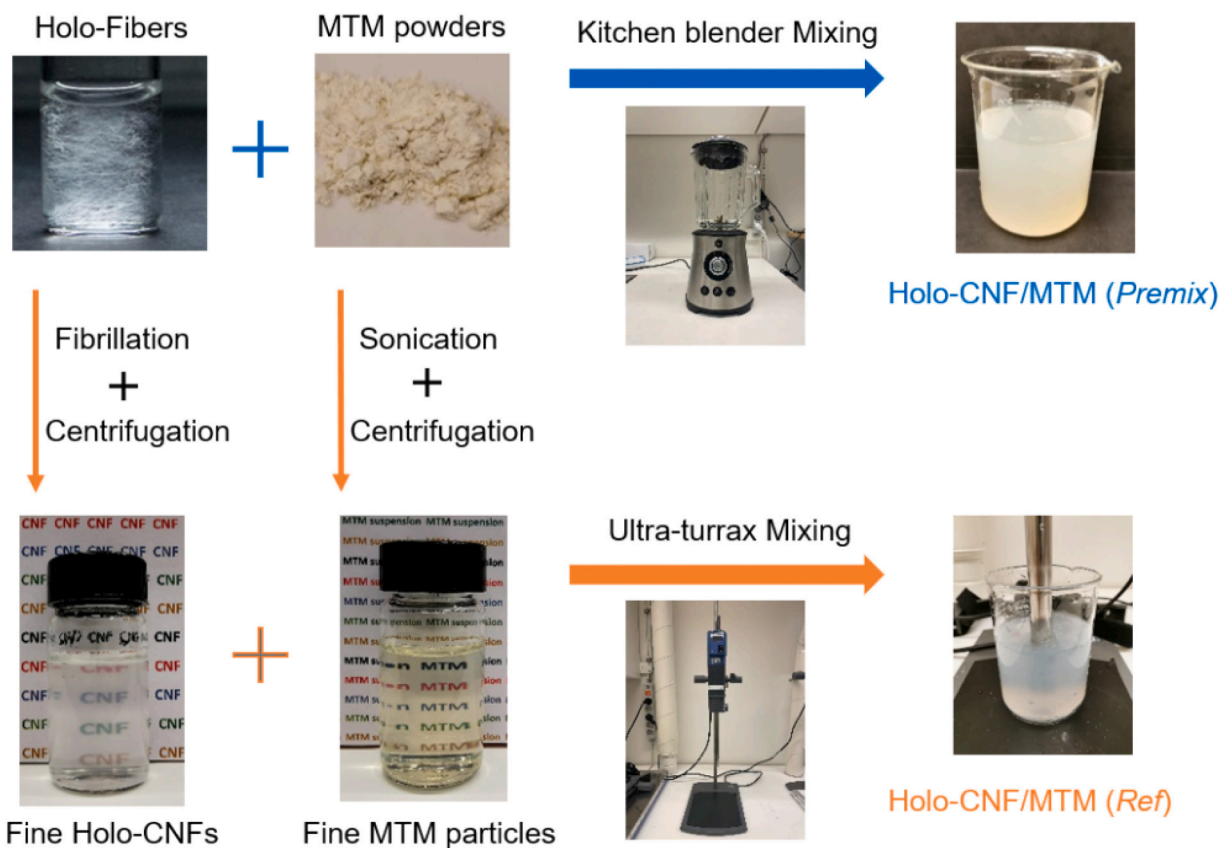


Fig. 1. Outline of *Premix* and *Ref* methods to obtain colloidal dispersions containing mixtures of CNF and MTM. Note that the dispersion concentration is different: *Premix* ( $\sim 0.6 \text{ wt\%}$ ), *Ref* ( $\sim 0.1 \text{ wt\%}$ ).

particles were successfully exfoliated into thin layers with an average thickness under 1–2 nm (Fig. 2a–f), as indicated by the height distribution profile 1 in Fig. 2h. These data are as good as those for fine Holo-CNFs and fine MTM particles (Fig. S2) which pass through a series of high-energy consuming processes in *Ref* method (Li et al., 2022; Yang et al., 2020). In addition, we also take the traditional *Enz-CNF* and fine MTM particle mixture samples as a comparison (Medina et al., 2019).

The use of hemicellulose-rich Holo-Fiber is important here, since the charged, water-swollen hemicellulose “coating” acts as a “spacer” between cellulose fibrils in the Holo-Fiber cell wall, which facilitates CNF fibrillation (Yang et al., 2021). Moreover, we hypothesize that since CNF from disintegrating Holo-Fibers will be present during MTM exfoliation, this CNF may prevent MTM aggregation after exfoliation. Consequently, fine MTM particles were formed and well dispersed in CNF colloids. As a comparison, conventional bleached kraft pulp fibers were blended with raw MTM particles using the same procedure, yet no CNF was obtained, and MTM was not exfoliated (Fig. 2g). According to the AFM height results (profile 2 in Fig. 2h), such aggregated MTM has a thickness of ~4 nm. Note that the embryonic concept of “co-grinding effect” of pulp fibers and mineral particles have been reported (Skuse, Phipps, & Larson, 2021; Svending, Phipps, & McLain, 2015), however, the function of fibrillated cellulose particles to assist the exfoliation of clay particles has not been analyzed. Also, in those studies, the final product is coarser microfibrillated celluloses and mineral particles, unable to form well-dispersed nanocomposites at the present nanoscale.

The high colloidal stability of CNF/MTM mixtures also allows longer storage time before use. The zeta potential and particle size of the colloids were determined by dynamic light scattering as listed in Table S1. Here, the stability of *Premix 50* and *Ref 50* (50 % MTM content) mixtures were determined by transmittance measurements (Fig. 3), with similar results when freshly made. After 10 days of storage, there is a small increase in turbidity for the bottom portion of the dispersions, because of aggregation. As comparison, a mixture based on fine *Enz-CNF* of lower charge and fine MTM (*Ref* method) has significantly lower transmittance due to aggregation effects. *Enz-CNF* is based on pulp pretreatment with hydrolyzing endoglucanase enzymes, and shows lower hemicellulose content and lower charge (Yang et al., 2020). We believe the higher hemicellulose content in CNF from Holo-Fibers with higher charge and

higher steric hindrance effects (from CNF surface hemicelluloses) provides improved dispersing effect for MTM particles. Note that 50 wt% MTM content is in a very high range among CNF/clay composites (George & Ishida, 2018).

Composite Films were prepared by vacuum filtration followed by hot-pressing (Liu & Berglund, 2012). The CNF/MTM ratio in these films was determined by TGA (Fig. S4 and Table S5). There is no obvious difference in surface morphology between *Premix* and *Ref* samples at the same MTM contents (Fig. S5), indicating the successful preparation of nanocomposites by the much simpler *Premix* method. While for each method, the surface structure becomes rougher at higher MTM loading, due to the increased porosity. The structure was characterized by WAXD, in which composite films were probed by X-ray with incident beam parallel to the film surface. The scattering patterns and corresponding 1D intensity profiles are shown in Fig. 4. CNF shows two diffraction arcs corresponding to 200 and 1–10/110 reflections centered in horizontal direction and a 004 arc in the vertical direction. These arc-like patterns indicate high in-plane orientation of CNFs. With increasing MTM contents from 0 to 50 wt%, the degree of orientation of CNFs increased from 0.78 to 0.83 for *Premix* samples and from 0.79 to 0.84 for *Ref* samples (Table S2). Platelets can improve the in-plane orientation of CNFs during vacuum filtration assembly (Mianehrow et al., 2020). Regarding the MTM peak intensity, it increases with increased MTM content, especially for 50 wt% sample. The estimated Scherrer size (tactoid thickness) is ~1.1 nm for *Premix* sample and ~1 nm for *Ref* sample. It means there are essentially no tactoids, instead single exfoliated MTM platelets are dominating. The Scherrer size obtained in our previous investigation (enzymatic pretreated CNF/MTM (Na<sup>+</sup>) system) was as high as 8–9 nm (Medina et al., 2019) and TEMPO-oxidized CNFs resulted in TOCN/MTM composites with a size of 2–4 nm (Li et al., 2022). The data suggest that the present MTM of *Premix* and *Ref* nanocomposites is better dispersed than in previous reports. The data are in support of the hypothesis that hemicellulose-rich CNFs facilitate MTM dispersion because of the charge and steric hindrance from the hemicellulose component.

The mechanical properties of CNF/MTM composite films were analyzed based on data from tensile tests, and the results are shown in Fig. 5. Composite films tend to show increasing Young’s modulus,

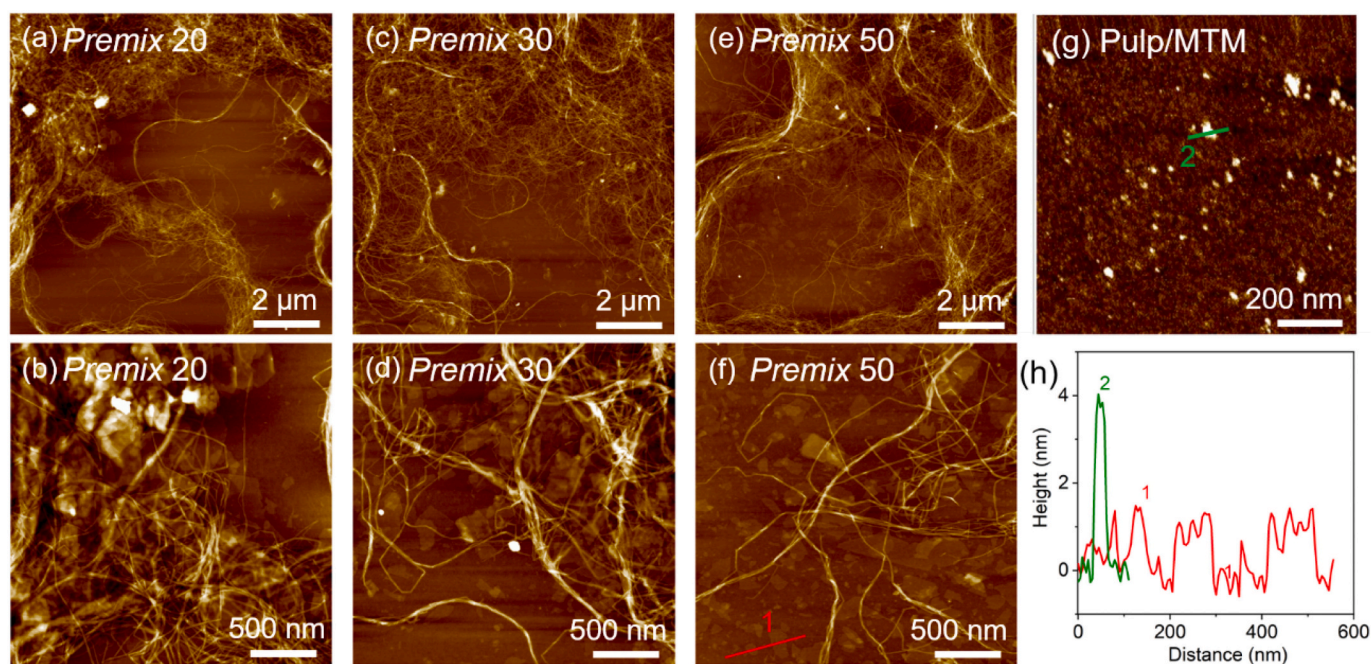


**Fig. 2.** AFM height images of Holo-CNF/MTM premix samples with 20%MTM (a, b), 30 % MTM (c, d) and 50%MTM (e, f); AMF height images of pulp fiber and MTM premix samples with 50 % MTM (g); Measured height for exfoliated MTM platelets (h): 1 *Premix*, and 2 bleached pulp + MTM Particles.

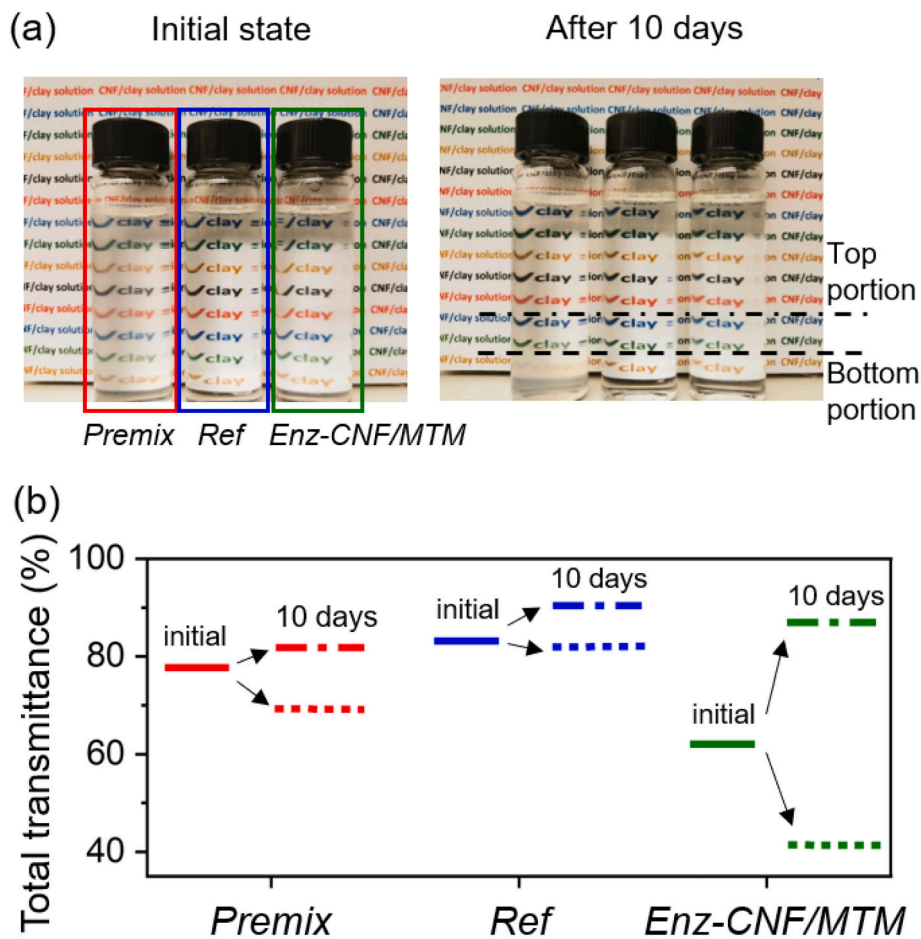


Fig. 3. (a) Photographs of *premix*, *Ref*, *Enz-CNF/MTM* suspensions (0.05 wt%) at 50 % MTM content in the initial state (freshly made) and after stored for 10 days. (b) Total optical transmittance of different dispersions when measured for top and bottom sections.

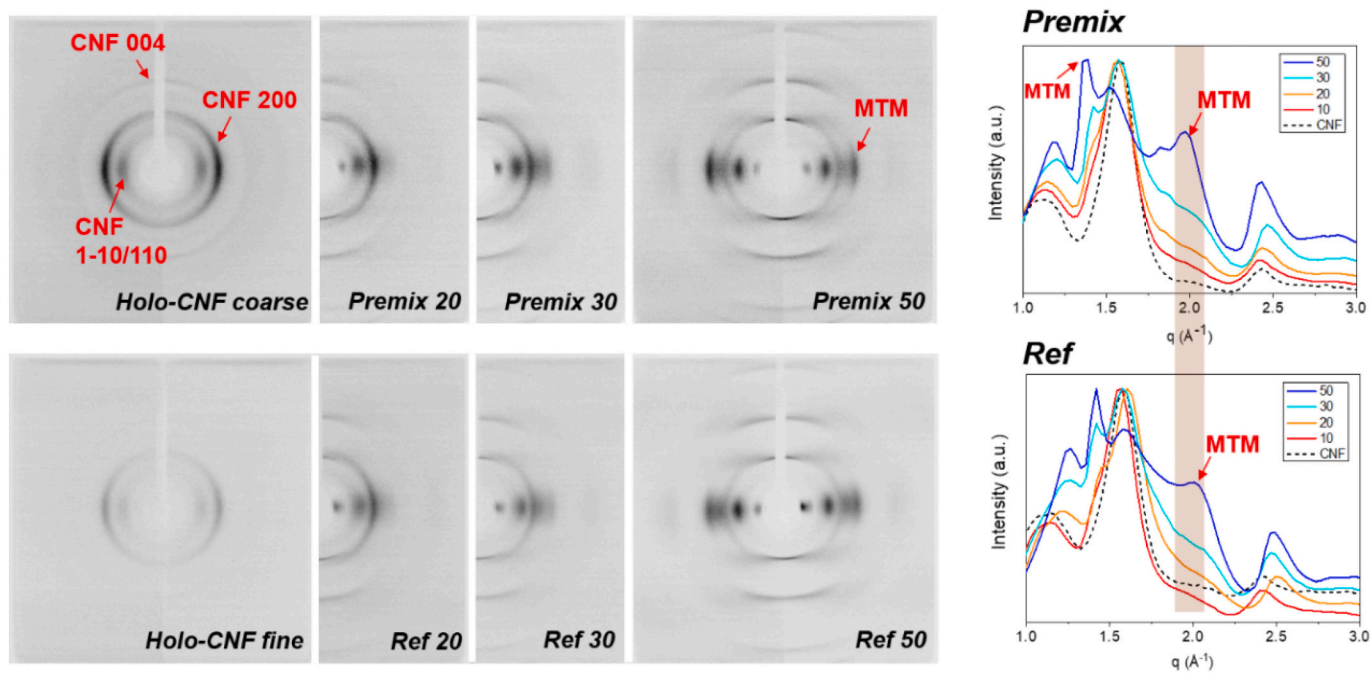


Fig. 4. 2D-WAXD patterns and corresponding 1D-curves of *Ref* and *Premix* samples.

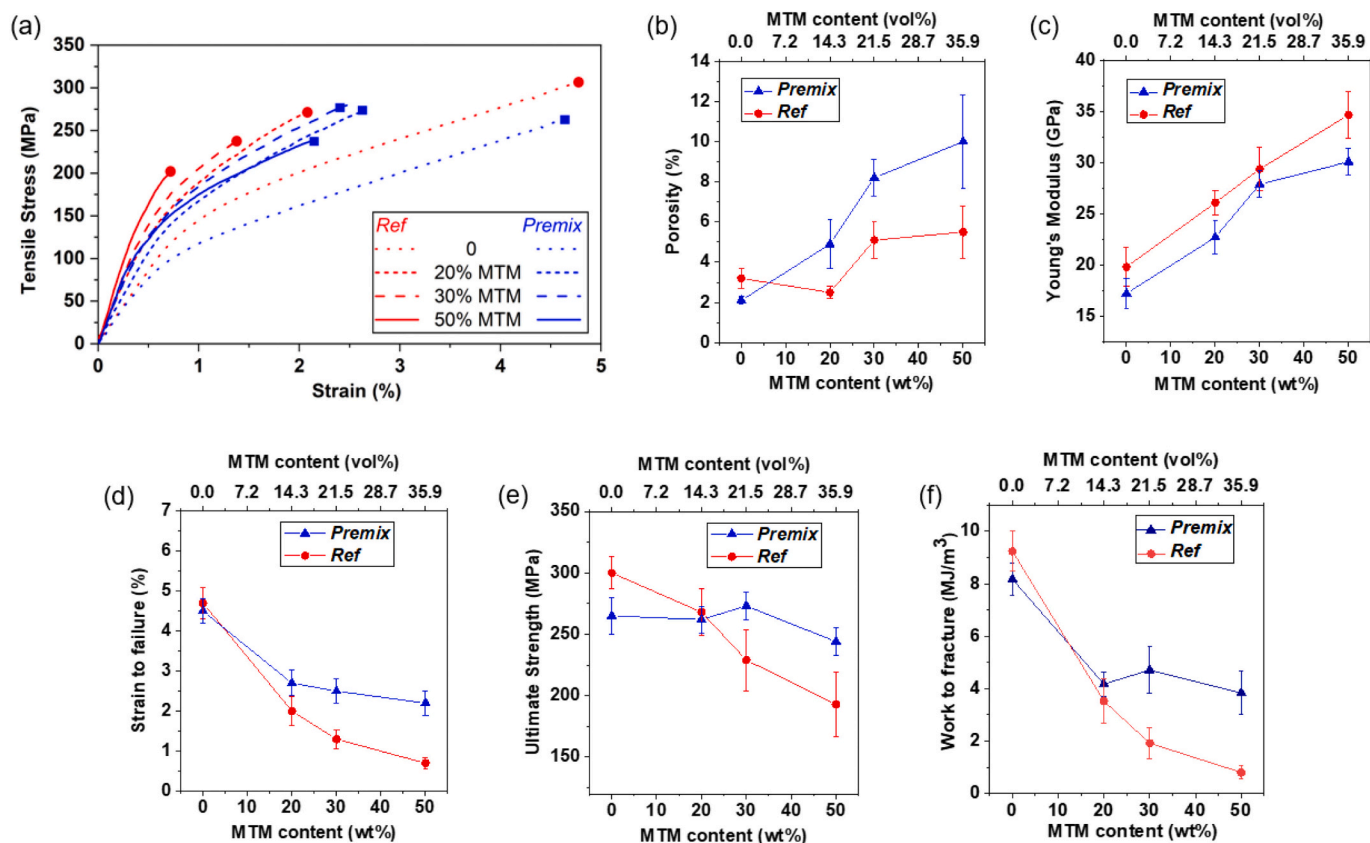


Fig. 5. Mechanical properties of Holo-CNF/MTM composite films prepared using *Premix* and *Ref* methods: a) Stress-strain curves, b) Porosity, c) Young's modulus, d) Strain to failure, e) Ultimate strength, f) Work to fracture (area under stress-strain curve). The detailed parameters are listed in Table S3.

decreasing strain at failure, decreasing work to fracture (area under stress-strain curve) and decreasing ultimate strength with increasing MTM content. The exception is strength data for *Premix* composites, which are not strongly influenced by MTM content (Fig. 5e). The high in-plane modulus of MTM platelets improves modulus of the composites, as high as 35 GPa at 50 wt% MTM (Fig. 5c). Moreover, the increased CNF in-plane orientation at higher MTM content will also contribute. The decreased strain to failure is related to strain magnification (Ziegel & Frensdorff, 1969). Compared with the CNF matrix, the high-stiffness MTM platelets are subjected to very small strain, which means that in many local regions (close to platelet edges, CNF-rich regions) the strain in the CNF matrix will be larger than the measured overall global strain. The higher the MTM content, the larger the concentration of local CNF strain compared with the macroscopic strain.

CNF/MTM composites have a layered structure which dominates fracture surfaces; the layers seem to fracture independently (Fig. 6). This may indicate limited interlayer adhesion, related to the filtering process and low content of out-of-plane CNFs. Fracture surfaces appear fairly similar for *Ref* and *Premix* nanocomposites. Neat CNF shows fracture surfaces with much lower roughness than for the composites. Ultimate composite fracture is likely to be initiated by local defects, possibly at specimen edges. At low MTM content, the fracture surfaces show short MTM/layer pull-out lengths which is usually related to high interfacial shear strength. At higher MTM content, the fracture surfaces show higher roughness, with layer pull-out lengths at much larger scale and such nanocomposites also show lower strain to failure. Possibly, the roughness is somewhat higher for the *Premix* nanocomposites. The pulled-out layers contain both MTM and CNF constituents. Note the increased porosity at higher MTM content (Fig. 5b) suggesting more and larger defects which may also influence the lower strain to failure (Fig. 5d) and ultimate strength values (Fig. 5e). When the CNF matrix content becomes very low, the adhesion between the CNF matrix and

MTM appears to be lowered. CNF fibrils are 4 nm or larger in diameter, whereas individual MTM thicknesses are only 1 nm. For low CNF content compositions, it is likely that weak CNF regions are present with lower than average local CNF content, higher nanoscale porosity and lowered effective interfacial shear strength.

The composite modulus  $E_{comp}$  (Fig. 5c) can be predicted by the classical “rule of mixtures” (Medina et al., 2019)

$$E_{comp} = E_{MTM}V_{MTM} + E_{CNF}V_{CNF} \quad (2)$$

where  $E_{MTM}$  and  $E_{CNF}$  are the moduli of MTM platelets and CNF matrix (film),  $V_{MTM}$  and  $V_{CNF}$  are the volume fractions of MTM and CNF, respectively. The effective  $E_{MTM}$  of *Premix* and *Ref* is 35.9 GPa and 41.8 GPa, respectively, as determined from the linear fit slope of the plot  $E_{comp}$  versus  $V_{MTM}$  in Fig. 5c. The higher porosity of *Premix* may explain its lower effective  $E_{MTM}$ . The value is much lower than theoretical  $E_{MTM}$ ; reasons have been discussed before (Medina et al., 2019) and include out-of-plane platelet orientation, porosity, aggregated platelet tactoids and imperfect CNF/MTM interface adhesion.

The comparison of data for *Premix* and *Ref* samples is interesting, especially at high MTM content, i.e. 50 wt%. Although *Premix* composite films have a much higher porosity compared to *Ref* (10 to 5.5 %), the former has significantly higher strain to failure (2.2 % vs 0.7 %), ultimate strength (244 MPa vs 193 MPa) and work to fracture (3.83 MJ/m<sup>3</sup> vs 0.81 MJ/m<sup>3</sup>). CNF fibril length is longer for the *Premix* method due to milder preparation method. Longer fibrils should form more efficient physical entanglements, which could improve the ultimate strength and strain at failure. High modulus is achieved by incorporating rigid clay platelets, with limited sacrifice of the original holocellulose CNF network ductility. Moreover, strength and modulus are higher than in most other CNF/MTM studies with CNFs of low hemicellulose content (Fig. 7). We suggest two major reasons: 1) *Premix* method results in

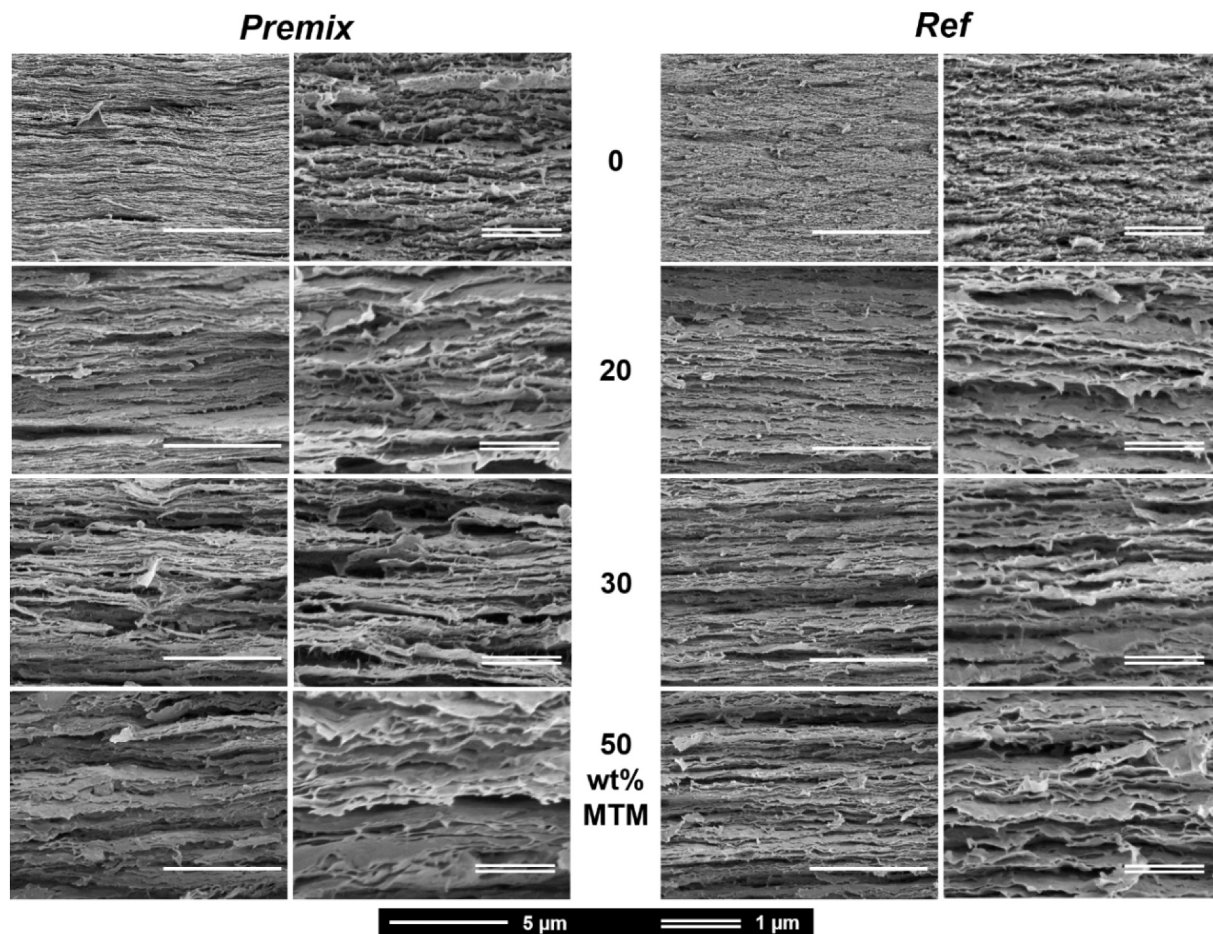


Fig. 6. SEM images of the fracture surface of holocellulose/MTM composites films prepared using *Premix* and *Ref* methods.

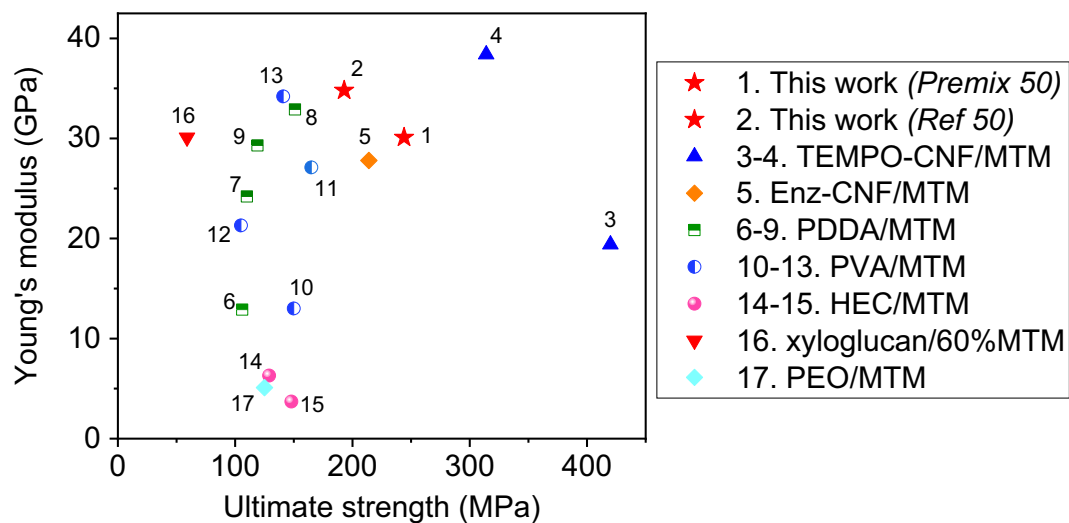


Fig. 7. Data for high MTM content nanocomposites (>50 wt%). Graphical comparison of the Young's modulus and ultimate strength of the present 1. *Premix* 50 and 2. *Ref* 50 samples with other hemicellulose-poor CNFs or polymer based composites with high clay content ( $\geq 50$  wt%): (3–4) TEMPO-CNF/MTM (Li et al., 2022; Wu et al., 2012), (5) Enzymatic pretreated-CNF/MTM (Medina et al., 2019), (6–9) PDDA/MTM (Walther et al., 2010), (10–13) PVA/MTM (Podsiadlo et al., 2007; Paul Podsiadlo et al., 2008; Walther et al., 2010), (14–15) HEC/MTM (Guo, Heng, Wang, Wang, & Jiang, 2016; Sehaqui, Kochumalayil, Liu, Zimmermann, & Berglund, 2013), (16) xyloglucan/MTM (Kochumalayil et al., 2013), and (17) PEO/MTM (Sehaqui et al., 2013). Detailed mechanical properties parameters are listed in Table S4.

improved MTM nanocomposite dispersion in the holocellulose CNF matrix, and 2) the high content anionic hemicellulose in the present CNF may combine good CNF colloidal dispersion with improved CNF-MTM adhesion in the form of shear strength, of importance for ultimate nanocomposite strength. The hemicellulose fraction is present as a CNF coating, which may increase the CNF-MTM contact area. In addition to these two major reasons, CNF length may be increased in the *Premix* method since less energy is used in mechanical disintegration. Other favorable strength data in Fig. 7 are data 3 and 4 from two previous investigations (Li et al., 2022; Wu, Saito, Fujisawa, Fukuzumi, & Isogai, 2012) using TEMPO-CNF and MTM. The data “3” is for specimens only 7–8  $\mu\text{m}$  in thickness, 2 mm in width and 10 mm in span length for tensile testing, which means that strength data are not really comparable with larger specimens. Here (data 1 and 2 in Fig. 7) we use  $5 \times 25$  mm and 30  $\mu\text{m}$  thickness. We have shown that smaller specimen size leads to higher strength data (Li et al., 2022). As specimen dimensions were changed from  $5 \times 25$  mm, 30  $\mu\text{m}$  thickness to  $2 \times 10$  mm and 7–8  $\mu\text{m}$  thickness, the strength for CNF/MTM with 31.5 wt% MTM went from 370 MPa to 470 MPa. The reason is that the probability for large defects is decreasing with smaller specimen size. When these small specimens were tested under dry conditions, rather than 50 % RH and room temperature, the strength increased further to 570 MPa (Li et al., 2022) It is concluded that comparisons of strength data must take specimen size and testing condition differences into account.

Compared to conventional *Ref* composite films, *Premix* composite films not only have improved ultimate strength and toughness with high MTM loading, but also significantly lower embodied energy (0.12 kWh/m<sup>2</sup> vs. 3.88 kWh/m<sup>2</sup>, energy to prepare the materials). As Fig. 8a and Table S6 shows, the centrifugation processes in *Ref* and traditional *Enz-CNF/MTM* method accounts for the majority of the energy demand, which are not present for *Premix*. Surprisingly, the energy demand for holocellulose CNFs using kitchen blender  $\approx 27$  % of the ultra-turrax mixing step before filtration. Fibrillation by kitchen blender requires significantly lower energy than microfluidizer use (0.02502 kWh/m<sup>2</sup> vs. 1.0467 kWh/m<sup>2</sup>). For *Enz-CNF/MTM* composites based on CNFs disintegrated by the use of microfluidizer, the total embodied energy is 4.92 kWh/m<sup>2</sup> (Fig. 8a). The radar plots (Fig. 8b) clearly show that the *Premix* method has very low energy demand combined with high mechanical performance, especially for the work to fracture (3.8 MJ/m<sup>3</sup>), which is much higher than for *Enz-CNF/MTM* (1.38 MJ/m<sup>3</sup>) and *Ref* method (0.8 MJ/m<sup>3</sup>). The *Premix* method for CNF/MTM composite films of high nanostructural control is of industrial interest, and large scale co-grinding of pulp fibers and minerals is already in industrial use (Skuse et al., 2021). The difference is that resulting composite structures are coarser than in the present approach, since low cost is a major criterion

for paper and packaging materials.

#### 4. Conclusions

The nanocomposite film processing of well-dispersed clay platelets in a CNF nanocellulose matrix usually requires several steps with high energy demand. Here, Holo-CNF/MTM hybrid composites are prepared by a simple “*Premix*” method using a low energy kitchen blender, where disintegration of hemicellulose-rich wood pulp fibers and clay exfoliation into individual platelets occurs simultaneously, followed by filtration and drying. Thus, the major energy-consuming steps of CNF and MTM nanoparticle preparation are avoided and the embodied process energy for a nanocomposite film is reduced by  $\sim 97$  %.

The use of hemicellulose-rich holocellulose wood pulp fibers combined with clay is of critical importance to low-energy defibrillation into well-preserved, colloidal stable Holo-CNF fibrils. The CNFs have sufficient anionic surface charge and steric hindrance from their hemicellulose coating (glucomannan-xylan). Furthermore, Holo-CNFs appear to have a “co-grinding” effect preventing MTM aggregation into tactoids after exfoliation. Consequently, the WAXD data showed nanocomposite structures of well-dispersed MTM platelets with an average thickness of 1–2 nm, even for 50 wt% MTM. The CNFs from this process also have fine “diameters” of 4–10 nm, based on AFM. The nanocomposite films show high in-plane orientation of MTM platelets (0.78–0.83), even at high MTM content (50 wt%). The commonly observed sacrifice of nanocomposite mechanical performance at high clay content, is much reduced due to the improved premixing strategy and corresponding reduction in MTM tactoid size. The Young’s modulus at 50 wt% MTM content is 30 GPa, ultimate strength 244 MPa and toughness 3.8 MJ/m<sup>3</sup> (area under stress-strain curve).

The present process reduces processing energy and reduces MTM tactoid size while providing strong in-plane orientation to provide excellent mechanical properties. CNF/MTM nanocomposites from natural resources can serve as transparent gas barriers, fire retardant layers and strong, stiff films and coatings.

#### CRediT authorship contribution statement

**Xuan Yang:** Conceptualization, Methodology, Formal analysis, Investigation, Data curation, Writing – original draft, Project administration. **Lengwan Li:** Conceptualization, Methodology, Formal analysis, Investigation, Data curation, Writing – original draft, Project administration. **Yoshiharu Nishiyama:** Methodology, Supervision, Writing – review & editing. **Michael S. Reid:** Methodology, Data curation. **Lars A. Berglund:** Writing – review & editing, Funding acquisition, Supervision,

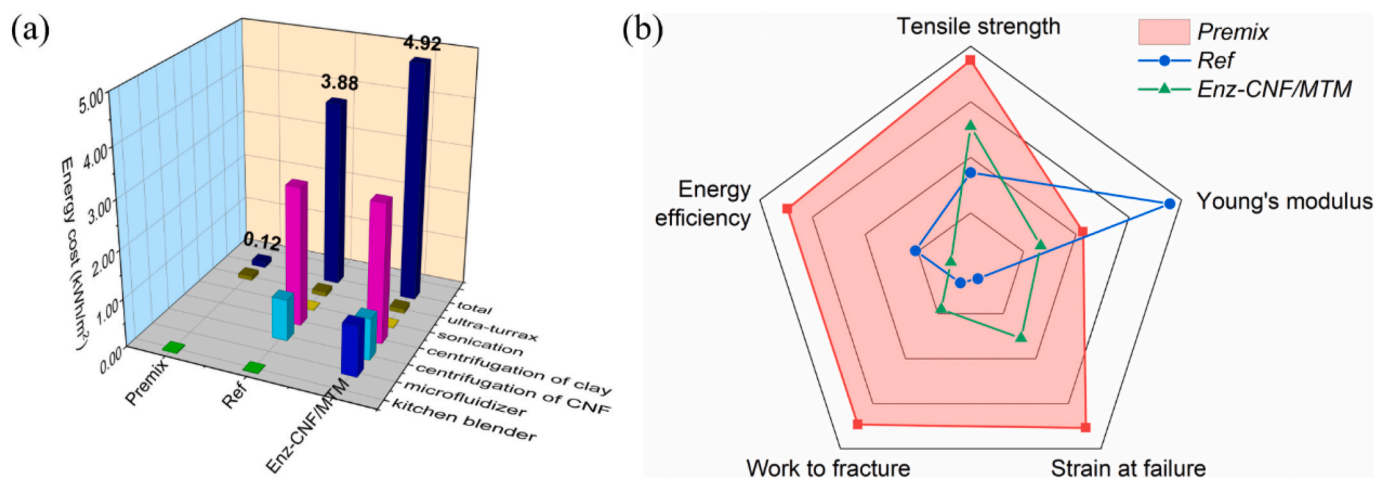


**Fig. 8.** (a) Comparison of the energy cost of each processing steps for *Premix*, *Ref* and *Enz-CNF/MTM* samples. (b) Radar plots comparing the performance and embodied energy cost of *Premix*, *Ref* and *Enz-CNF/MTM* samples with 50 % MTM.

Investigation.

### Declaration of competing interest

The authors declare that they have no known competing financial interests or personal relationships that could have appeared to influence the work reported in this paper.

### Data availability

Data will be made available on request.

### Acknowledgments

The authors acknowledge funding from the Swedish Research Council, project 2021-03882, and the Knut and Alice Wallenberg Foundation through Wallenberg Wood Science Center and the Bio-composites program at the KTH Royal Institute of Technology. X.Y. is thankful for the funding from National Natural Science Foundation of China (Grants NO. 22278359 and 22108244), “Pioneer” and “Leading Goose” R&D Program of Zhejiang (Grant NO. 2022C01234). The authors acknowledge Dr. Andrew Inge (MMK, Stockholm University) for the assistance of WAXD measurements.

### Appendix A. Supplementary data

Supplementary data to this article can be found online at <https://doi.org/10.1016/j.carbpol.2023.120788>.

### References

- Alves, L., Ramos, A., Rasteiro, M. G., Vitorino, C., Ferraz, E., Ferreira, P. J. T., Puertas, M. L., & Gamelas, J. A. F. (2022). Composite films of nanofibrillated cellulose with sepiolite: Effect of preparation strategy. *Coatings*, *12*(3), 303.
- Bee, S.-L., Abdullah, M. A. A., Bee, S.-T., Sin, L. T., & Rahmat, A. R. (2018). Polymer nanocomposites based on silylated-montmorillonite: A review. *Progress in Polymer Science*, *85*, 57–82.
- Carosio, F., Kochumalayil, J., Cuttica, F., Camino, G., & Berglund, L. (2015). Oriented clay nanopaper from biobased components—mechanisms for superior fire protection properties. *ACS Applied Materials & Interfaces*, *7*(10), 5847–5856.
- Carosio, F., Medina, L., Kochumalayil, J., & Berglund, L. A. (2021). Green and fire resistant nanocellulose/hemicellulose/clay foams. *Advanced Materials Interfaces*, *8*(18), 2101111.
- Chen, C., Kuang, Y., Zhu, S., Burgert, I., Keplinger, T., Gong, A., & Hu, L. (2020). Structure–property–function relationships of natural and engineered wood. *Nature Reviews Materials*, *5*(9), 642–666.
- Gao, X., Tian, R., Liu, X., Zhu, H., Tang, Y., Xu, C., & Li, H. (2019). Specific ion effects of  $\text{Cu}^{2+}$ ,  $\text{Ca}^{2+}$  and  $\text{Mg}^{2+}$  on montmorillonite aggregation. *Applied Clay Science*, *179*, Article 105154.
- George, J., & Ishida, H. (2018). A review on the very high nanofiller-content nanocomposites: Their preparation methods and properties with high aspect ratio fillers. *Progress in Polymer Science*, *86*, 1–39.
- Gim, J., Schnitzer, N., Otter, L. M., Cui, Y., Motreuil, S., Marin, F., & Hovden, R. (2019). Nanoscale deformation mechanics reveal resilience in nacre of *Pinna nobilis* shell. *Nature Communications*, *10*(1), 4822.
- Guo, T., Heng, L., Wang, M., Wang, J., & Jiang, L. (2016). Robust underwater oil-repellent material inspired by columnar nacre. *Advanced Materials*, *28*(38), 8505–8510.
- Guo, Y. X., Liu, J. H., Gates, W. P., & Zhou, C. H. (2020). Organo-modification of montmorillonite. *Clays and Clay Minerals*, *68*(6), 601–622.
- Hajizadeh, Z., Taheri-Ledari, R., & Asl, F. R. (2022). 3. Identification and analytical methods. In A. Maleki (Ed.), *Heterogeneous micro and nanoscale composites for the catalysis of organic reactions* (pp. 33–51). Elsevier.
- Henriksson, M., Henriksson, G., Berglund, L. A., & Lindström, T. (2007). An environmentally friendly method for enzyme-assisted preparation of microfibrillated cellulose (MFC) nanofibers. *European Polymer Journal*, *43*(8), 3434–3441.
- Kochumalayil, J. J., Morimune, S., Nishino, T., Ikkala, O., Walther, A., & Berglund, L. A. (2013). Nacre-mimetic clay/xyloglucan bionanocomposites: A chemical modification route for hygromechanical performance at high humidity. *Biomacromolecules*, *14*(11), 3842–3849.
- Kontturi, E., Laaksonen, P., Linder, M. B., Nonappa, Gröschel, A. H., Rojas, O. J., & Ikkala, O. (2018). Advanced materials through assembly of nanocelluloses. *Advanced Materials*, *30*(24), 1703779.
- Li, L., Maddalena, L., Nishiyama, Y., Carosio, F., Ogawa, Y., & Berglund, L. A. (2022). Recyclable nanocomposites of well-dispersed 2D layered silicates in cellulose nanofibril (CNF) matrix. *Carbohydrate Polymers*, *279*, Article 119004.
- Liu, A., & Berglund, L. A. (2012). Clay nanopaper composites of nacre-like structure based on montmorillonite and cellulose nanofibers—Improvements due to chitosan addition. *Carbohydrate Polymers*, *87*(1), 53–60.
- Liu, A., Walther, A., Ikkala, O., Belova, L., & Berglund, L. A. (2011). Clay nanopaper with tough cellulose nanofiber matrix for fire retardancy and gas barrier functions. *Biomacromolecules*, *12*(3), 633–641.
- Luz, G. M., & Mano, J. F. (2009). Biomimetic design of materials and biomaterials inspired by the structure of nacre. *Philosophical Transactions of the Royal Society A: Mathematical, Physical and Engineering Sciences*, *367*(1893), 1587–1605.
- Manevitch, O. L., & Rutledge, G. C. (2004). Elastic properties of a single lamella of montmorillonite by molecular dynamics simulation. *The Journal of Physical Chemistry B*, *108*(4), 1428–1435.
- Medina, L., Nishiyama, Y., Daicho, K., Saito, T., Yan, M., & Berglund, L. A. (2019). Nanostructure and properties of nacre-inspired Clay/Cellulose Nanocomposites—Synchrotron X-ray scattering analysis. *Macromolecules*, *52*(8), 3131–3140.
- Mianehrow, H., Lo Re, G., Carosio, F., Fina, A., Larsson, P. T., Chen, P., & Berglund, L. A. (2020). Strong reinforcement effects in 2D cellulose nanofibril–graphene oxide (CNF–GO) nanocomposites due to GO-induced CNF ordering. *Journal of Materials Chemistry A*, *8*(34), 17608–17620.
- Podsiadlo, P., Kaushik, A. K., Arruda, E. M., Waas, A. M., Shim, B. S., Xu, J., & Kotov, N. A. (2007). Ultrastrong and stiff layered polymer nanocomposites. *Science*, *318*(5847), 80–83.
- Podsiadlo, P., Kaushik, A. K., Shim, B. S., Agarwal, A., Tang, Z., Waas, A. M., & Kotov, N. A. (2008). Can nature’s design be improved upon? High strength, transparent nacre-like nanocomposites with double network of sacrificial cross links. *The Journal of Physical Chemistry B*, *112*(46), 14359–14363.
- Saito, T., Kimura, S., Nishiyama, Y., & Isogai, A. (2007). Cellulose nanofibers prepared by TEMPO-mediated oxidation of native cellulose. *Biomacromolecules*, *8*(8), 2485–2491.
- Scherrer, P. (1918). Nachrichten von der Gesellschaft der Wissenschaften zu Göttingen. *Mathematisch-Physikalische Klasse*, *2*, 98–100.
- Sehaqui, H., Kochumalayil, J., Liu, A., Zimmermann, T., & Berglund, L. A. (2013). Multifunctional nanoclay hybrids of high toughness, thermal, and barrier performances. *ACS Applied Materials & Interfaces*, *5*(15), 7613–7620.
- Skuse, D., Phipps, J., & Larson, T. (2021). Co-ground mineral/microfibrillated cellulose composite materials: Recycled fibers, engineered minerals, and new product forms. *Tappi Journal*, *20*(1), 49–58.
- Vanderfleet, O. M., & Cranston, E. D. (2021). Production routes to tailor the performance of cellulose nanocrystals. *Nature Reviews Materials*, *6*(2), 124–144.
- Walther, A., Bjuhager, I., Malho, J.-M., Pere, J., Ruokolainen, J., Berglund, L. A., & Ikkala, O. (2010). Large-area, lightweight and thick biomimetic composites with superior material properties via fast, economic, and green pathways. *Nano Letters*, *10*(8), 2742–2748.
- Walther, A., Bjuhager, I., Malho, J.-M., Ruokolainen, J., Berglund, L., & Ikkala, O. (2010). Supramolecular control of stiffness and strength in lightweight high-performance nacre-mimetic paper with fire-shielding properties. *Angewandte Chemie International Edition*, *49*(36), 6448–6453.
- Wang, J., Cheng, Q., Lin, L., & Jiang, L. (2014). Synergistic toughening of bioinspired poly(vinyl alcohol)–clay–nanofibrillar cellulose artificial nacre. *ACS Nano*, *8*(3), 2739–2745.
- Wu, C. N., Saito, T., Fujisawa, S., Fukuzumi, H., & Isogai, A. (2012). Ultrastrong and high gas-barrier nanocellulose/clay-layered composites. *Biomacromolecules*, *13*(6), 1927–1932.
- Yang, X., Berthold, F., & Berglund, L. A. (2019). High-density molded cellulose fibers and transparent biocomposites based on oriented holocellulose. *ACS Applied Materials & Interfaces*, *11*(10), 10310–10319.
- Yang, X., Jungstedt, E., Reid, M. S., & Berglund, L. A. (2021). Polymer films from cellulose Nanofibrils—Effects from interfibrillar interphase on mechanical behavior. *Macromolecules*, *54*(9), 4443–4452.
- Yang, X., Reid, M. S., Olsen, P., & Berglund, L. A. (2020). Eco-friendly cellulose nanofibrils designed by nature: Effects from preserving native state. *ACS Nano*, *14*(1), 724–735.
- Zhang, Y., Tian, J., Zhong, J., & Shi, X. (2018). Thin nacre-biomimetic coating with super-anticorrosion performance. *ACS Nano*, *12*(10), 10189–10200.
- Zhou, S. Q., Niu, Y. Q., Liu, J. H., Chen, X. X., Li, C. S., Gates, W. P., & Zhou, C. H. (2022). Functional montmorillonite/polymer coatings. *Clays and Clay Minerals*, *70*(2), 209–232.
- Ziegel, K. D., Frensdorff, H. K., & Fogiel, A. W. (1969). Strain magnification in polymer composites. *Journal of Applied Polymer Science*, *13*(5), 867–869.
- Svending, P., Phipps, J., & McLain, L. (2015). *Microfibrillated Cellulose – Mineral Composites for Paper and Paperboard Applications*. TAPPI PaperCon 2015, Atlanta, Georgia.